

Three- to Two-Dimensional Transition of the Electronic Structure in CaFe_2As_2 - parent compound for an iron arsenic high temperature superconductor

Chang Liu,¹ Takeshi Kondo,¹ Ni Ni,¹ A. D. Palczewski,¹ A. Bostwick,² G. D. Samolyuk,¹ R. Khasanov,³ M. Shi,⁴ E. Rotenberg,² S. L. Bud'ko,¹ P. C. Canfield,¹ and A. Kaminski¹

¹*Ames Laboratory and Department of Physics and Astronomy, Iowa State University, Ames, Iowa 50011, USA*

²*Advanced Light Source, Berkeley National Laboratory, Berkeley, California 94720, USA*

³*Laboratory for Muon Spin Spectroscopy, Paul Scherrer Institut, CH-5232 Villigen PSI, Switzerland*

⁴*Swiss Light Source, Paul Scherrer Institute, 5232 Villigen PSI, Switzerland*

(Dated: November 24, 2018)

We use angle-resolved photoemission spectroscopy (ARPES) to study the electronic properties of CaFe_2As_2 - parent compound of a pnictide superconductor. We find that the structural and magnetic transition is accompanied by a three- to two-dimensional (3D-2D) crossover in the electronic structure. Above the transition temperature (T_s) Fermi surfaces around Γ and X points are cylindrical and quasi-2D. Below T_s the former becomes a 3D ellipsoid, while the latter remains quasi-2D. This finding strongly suggests that low dimensionality plays an important role in understanding the superconducting mechanism in pnictides.

PACS numbers: 79.60.-i, 74.25.Jb, 74.70.Dd

The dimensionality of electronic structure plays an important role in the superconductivity of solids. The cuprate superconductors have the highest known transition temperatures and they have quasi two dimensional (2D) electronic structure. In contrast, the borocarbides [1], another class of relatively high transition temperature superconductors, have a strictly three dimensional (3D) electronic structure [2]. The situation in the newly discovered iron arsenic high temperature superconductors is less clear. Both $R\text{FeAsO}$ ($R1111$, R being the rare earth element) [3] and $A\text{Fe}_2\text{As}_2$ ($A122$, A being Ca, Sr, Ba) [4] have strongly layered structures, with the iron-arsenic layers believed to be mainly responsible for the electronic properties and superconductivity. The $A122$ family share the same ThCr_2Si_2 structure as the borocarbides and both display interesting interplay between magnetism and superconductivity. Some band structure calculations predict strong k_z dispersion and 3D Fermi surfaces (FSs) [6] in the magnetic state of the parent compounds, however so far this has not been observed by angle-resolved photoemission spectroscopy (ARPES) [7, 8, 9, 10, 11, 12, 13]. On the other hand, a number of physical properties display an anisotropy that is a few orders of magnitude smaller than that found in the cuprates [14, 15, 16], which hints at a strong hopping between the layers. In terms of the pairing mechanism, most theoretical models depend on nesting between the Γ - and $X(M)$ -pockets [17, 18], for which the dimensionality of the FSs is very important.

The parent compounds of the two iron pnictide families undergo a tetragonal-to-orthorhombic (Tet-Ortho) structural/magnetic transition at elevated temperatures [14, 19]. Superconductivity appears in the $A122$ materials when the high temperature Tet-phase is stabilized down to low enough temperatures (usually by doping with K in a Ba position or Co substitution for Fe

which lowers the transition temperature) [20]. Determining the differences between these phases is key to gaining a full understanding and control of the superconductivity in the iron-pnictides. In particular, CaFe_2As_2 shows a first order Tet-Ortho transition with a transition temperature ($160 \sim 170\text{K}$) depending on the growth method [21, 22, 23]. Superconductivity is found when moderate (possibly not purely hydrostatic) pressure is applied [24], or by doping with cobalt [22] or sodium [23]. Such a rich phase diagram makes CaFe_2As_2 an ideal system for studying the electronic properties of the parent compounds. In this Letter we present ARPES data which demonstrates that the electronic structure in the parent compound of the $A122$ iron arsenic family undergoes a 3D to 2D crossover associated with the structural/magnetic transition. The cylindrical, quasi-2D FS surrounding the Γ -point becomes highly dispersive (3D) and forms an ellipsoid upon cooling below the transition temperature into the Ortho-phase. The observation of the 3D FS is consistent with recent results from quantum oscillation measurements [25, 26]. The FSs around the X-pocket remain quasi-2D and unaffected by the structural transition.

Plate like single crystals of CaFe_2As_2 were grown out of a FeAs flux as well as Sn flux using conventional high-temperature solution growth techniques [21] with typical dimensions ranging from $2 \times 2 \text{ mm}^2$ up to $10 \times 10 \text{ mm}^2$. Following the growth the samples were annealed at 500°C for 24 hours. Resistivity measurements showed a first-order Tet-Ortho transition at $\sim 160\text{K}$ for the FeAs flux grown samples and $\sim 170\text{K}$ when using Sn flux. The ARPES measurements are performed at beam lines 10.0.1 and 7.0.1 of the Advanced Light Source (ALS), Berkeley, California, and the SIS beam line of the Swiss Light Source, Switzerland. Energy resolution was set at $20 \sim 30\text{meV}$, vacuum conditions were better than

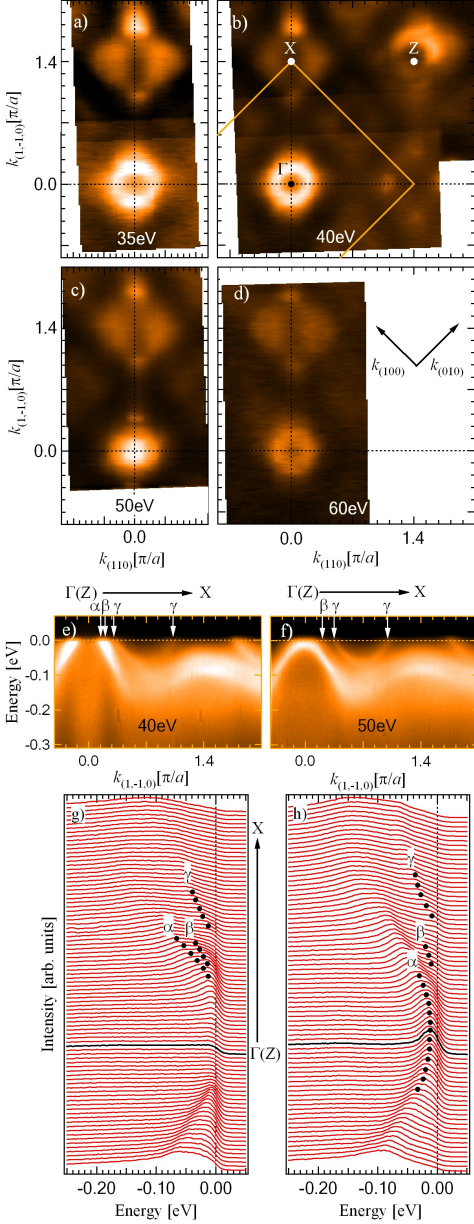


FIG. 1: (color online) Fermi surface maps of CaFe_2As_2 low temperature orthorhombic phase ($T = 12\text{K}$) for a few photon energies. (a)-(d) ARPES intensity integrated within 10 meV about μ for $h\nu = 35, 40, 50$ and 60eV , respectively. Bright areas mark the location of the Fermi surfaces. (e)-(f) Band dispersion data along the Γ -X direction for $h\nu = 40$ and 50eV . α, β, γ correspond to different bands that cross μ . (g)-(h) Energy distribution curves (EDCs) for data in panels (e)-(f) over the same k range.

5×10^{-11} torr. All samples were cleaved *in situ* along the (001) plane, yielding mirror-like, clean surfaces. Lattice constant values from Ref. [27] are used to determine the k -space positions. The high symmetry points X and Z for both two phases are defined to be $(\pi/a, \pi/a(b), 0)$ and $(0, 0, 2\pi/c)$, respectively, with k_x ($k_{(100)}$) and k_y ($k_{(010)}$)

axes along the Fe-As bonds.

FS maps of CaFe_2As_2 obtained at several different photon energies in the Ortho-phase are shown in Fig. 1 along with ARPES intensity plots and energy distribution curves (EDCs). Varying the photon energy in ARPES effectively changes the momentum offset along the direction perpendicular to the sample surface (in our case this direction corresponds to k_z - perpendicular to the Fe-As layers) [28, 29]. The striking feature of Fig. 1 is that the dispersion of one of the bands that form the “ Γ -pocket” (Fermi contour around the zone center $k_x = k_y = 0$) changes dramatically with photon energy. At $h\nu = 40\text{eV}$, three different bands α, β and γ cross the chemical potential (μ) as seen in Figs. 1(e), 1(g) and this gives rise to three FS sheets. The γ -band crosses μ again near the X-point, forming a characteristic flower shape of the X-pocket. The other two bands (α, β) are relatively close to each other. They form two hole pockets around Γ . Similar behavior has been reported in $\text{Ba}_{1-x}\text{K}_x\text{Fe}_2\text{As}_2$ [7, 8, 30, 31, 32]. However, at $h\nu = 50\text{eV}$, the top of the α band is located below μ and the corresponding α -pocket disappears. The β - and γ -pockets continue to cross μ at about the same k_F as for 40eV photons [Figs. 1(c), 1(f) and 1(h)]. These data conclusively demonstrate that the electronic structure in the Ortho-phase of CaFe_2As_2 is 3D. On the other hand, no obvious change is seen for the X-pocket at these 4 energies.

A comprehensive study of the evolution of the Γ - and X-pocket with different incident photon energies is shown in Fig. 2 for the Ortho-phase of CaFe_2As_2 . The photon energy ranges from 35 to 105eV. The FS map along the k_z direction is shown in Fig. 2(a) over a range corresponding to several Brillouin zones. The α Fermi pocket forms an ellipsoid centered at Γ in the respective Brillouin zones with a $4\pi/c$ periodicity. It should be noted that the observation of k_z dispersion with such periodicity clearly demonstrates that ARPES data from these samples reveals intrinsic, bulk electronic properties. In Fig. 2(b) we extract the Fermi crossing momenta (k_{FS}) from the momentum distribution curve (MDC) peaks at μ for each photon energy. It is clear that only the α -band (black solid dots) but not the β - and γ -bands show a strong k_z dispersion. Almost no dispersion of the X-pocket is observed, which indicates its quasi 2D nature. The consistency of this map with that of Fig. 1 is better seen at Figs 2(c)-2(e) where ARPES intensity maps are shown for 3 high symmetry points. At $h\nu = 58\text{eV}$ ($k_z = 16\pi$) the α -band does not cross μ , while at $h\nu = 80$ and 41eV ($k_z = 18\pi$ and 14π) all three bands form Fermi pockets.

Now we turn our attention to the high temperature Tet-phase of CaFe_2As_2 . We demonstrate in Fig. 3 the 2D character of the band structure in the Tet-phase. Panel 3(a) shows the FS map at $h\nu = 100\text{eV}$. An arrow represents the Γ -Z direction along which data in panels (d) and (e) were obtained. Schematic arrangement of the Brillouin zones along in-plane and out-of-plane directions for

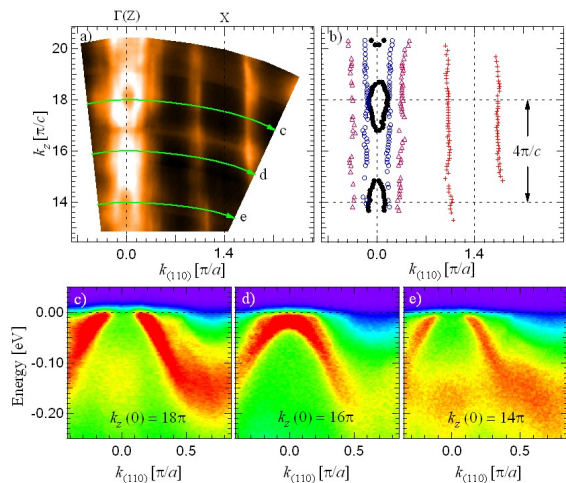


FIG. 2: (color online) k_z dispersion data for CaFe_2As_2 low temperature orthorhombic phase ($T = 40\text{K}$). (a) k_z dispersion data obtained by plotting ARPES intensity integrated within 10 meV about μ as a function of $k_{(110)}$ and the energy of the incident photons (which corresponds to different values of k_z). The photon energy range used was from 35 to 105 eV. (b) Fermi momentum k_F was extracted from the data in panel (a) using the peak positions of the MDCs. (c)-(e) Band dispersion data along the Γ -X direction for $k_z = 18, 16$ and 14π at $k_{(110)} = 0$ (corresponding to photon energies of $h\nu = 80, 58$ and 41eV , respectively). The locations of these cuts are marked by green lines in panel (a).

the Tet-phase are shown in panels 3(b) and 3(c). Panels 3(d) and 3(e) presents the actual k_z intensity data integrated within 10 meV about μ as a function of k_z and k_x and the band dispersion extracted using MDC peaks respectively. The photon energy range used here is 80 to 190eV, which corresponds to $18\pi \leq k_z \leq 25\pi$. The most important observation here is that the bands around Γ cross μ at *all* k_z s measured, no apparent k_z dispersion is visible. For further clarification, in panels 3(f)-3(i) we show ARPES intensity maps divided by the resolution convoluted Fermi function for $k_z = 18, 19, 20$ and 21π respectively. The band crosses μ for all these k -points, in clear contrast with the situation for the low temperature Ortho-phase. The data in Fig. 3 is consistent with a quasi-2D nature of the FS in the high temperature Tet-phase of CaFe_2As_2 .

In Fig. 4 we directly compare the band dispersion of low and high temperature phase for the two k_z values that correspond to high symmetry points. The data is taken along Γ -X direction on the same sample under exactly the same experimental conditions to avoid possible complications due to scattering matrix elements or polarization of incident photons. Though the data in Fig. 4 is taken from different samples and beam lines than that in Fig. 2, the 3D nature of the low temperature Ortho-phase reproduces nicely. At high temperature we divided the data by the resolution convoluted Fermi func-

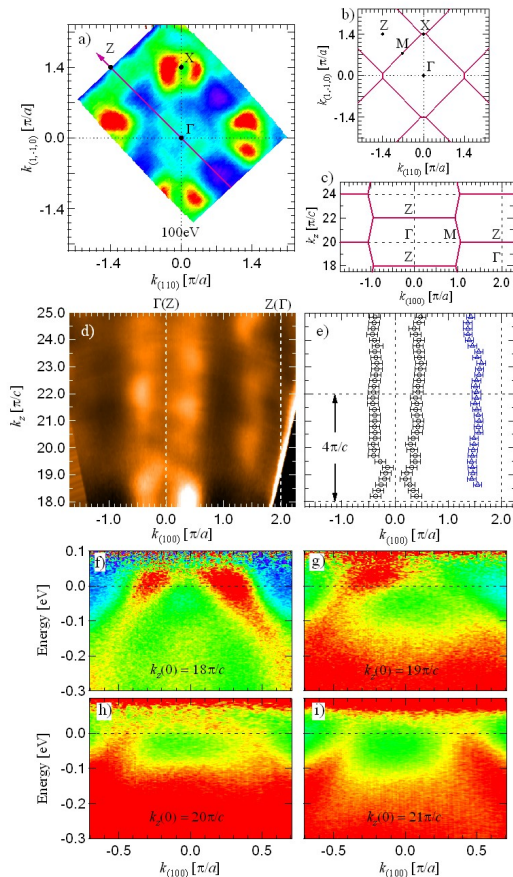


FIG. 3: (color online) k_z dispersion data for CaFe_2As_2 in the high temperature tetragonal phase ($T = 200\text{K}$). (a) FS maps for $h\nu = 100\text{eV}$. (b) Brillouin zone structure in the k_x - k_y plane for the measured range. (c) Same as (b) but in the k_x - k_z (Γ -Z) plane. (d) k_z dispersion data parallel to Γ -M (marked by magenta arrow in panel (a)). The corresponding photon energy range was 80 to 190 eV. (e) Fermi crossing momenta k_{FS} extracted from the data in panel (d). (f)-(i) Band dispersion data along a direction parallel to Γ -M for $k_z = 18, 19, 20$ and 21π at $k_x = 0$ (corresponding to incident photon energies of $h\nu = 80, 89, 99$ and 110eV). The data was divided by the resolution convoluted Fermi function to reveal the dispersion in the vicinity of μ .

tion to better see the location of the band in the proximity of μ . At low temperature this is not necessary, as the width of the Fermi edge is much sharper than the leading edge of the peaks, band crossings are clearly visible. At $T = 200\text{K}$, the α -band crosses μ at both points ($k_z = 16\pi$ and $k_z = 18\pi$ - Figs. 4(a) and 4(b)). At low temperature in the Ortho-phase, the same band crosses μ at $k_z = 18\pi$ (Fig. 4(d)), but is located several tens of meV below μ at $k_z = 16\pi$ (Fig. 4(c)). This may be the origin of the sudden drop in the electric resistivity found by transport measurements when the material is heated above the transition temperature [21, 23].

In conclusion, we have measured the in-plane and

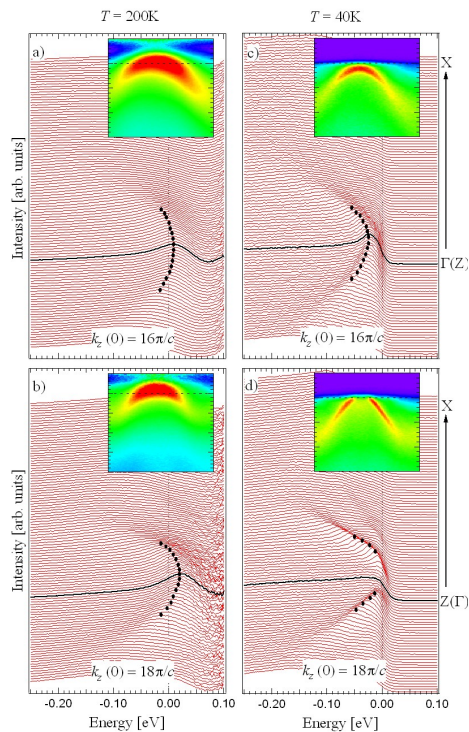


FIG. 4: (color online) Direct comparison of band dispersions for low and high temperature phase of CaFe_2As_2 . Each panel shows the EDCs in vicinity of the Γ -point (black solid curve) along $k_{(110)}$ direction. High temperature data was divided by the resolution convoluted Fermi function to reveal dispersion in the vicinity of μ . Insets show the corresponding plot of band dispersion. Data was obtained at temperatures and momenta indicated in the panels.

out-of-plane band dispersion for both the orthorhombic (Ortho) and tetragonal (Tet) phase of the iron arsenic A122 parent compound CaFe_2As_2 . A number of theoretical models of the pairing mechanism and magnetic ordering in these materials are based on nesting between different sheets of the Fermi surface [17, 18]. Our results demonstrate that some FS sheets are indeed three dimensional, therefore put significant constrains on possible nesting scenarios, since the degree of nesting will strongly depend on the dimensionality of the FSs. Our finding also has important implications for understanding a number of other physical properties such as the anisotropy in electrical and thermal conductivity [33] which depend on the dimensionality of the electronic structure.

We thank J. Schmalian, M. A. Tanatar and Rafael Fernandes for insightful discussions and staff at SLS and

ALS for excellent instrumentation support. Ames Laboratory was supported by the Department of Energy - Basic Energy Sciences under Contract No. DE-AC02-07CH11358. ALS is operated by the US DOE under Contract No. DE-AC03-76SF00098.

- [1] L. C. Gupta, *Advances in Physics*, **55**, 691 (2006).
- [2] P. Starowicz *et al.*, *Phys. Rev. B* **77**, 134520 (2008).
- [3] Y. Kamihara, T. Watanabe, M. Hirano, and H. Hosono, *J. Am. Chem. Soc.* **130**, 3296 (2008).
- [4] Marianne Rotter, Marcus Tegel, and Dirk Johrendt, *Phys. Rev. Lett.* **101**, 107006 (2008).
- [5] D.J. Singh *et al.*, arXiv:0810.2682 (2008) and references therein.
- [6] Fengjie Ma *et al.*, arXiv:0806.3526v2 (2008).
- [7] H. Ding *et al.*, *Europhys. Lett.* **83**, 47001 (2008).
- [8] Lin Zhao *et al.*, *Chin. Phys. Lett.* **25**, 4402 (2008).
- [9] L. Wray *et al.*, *Phys. Rev. B* **78**, 184508 (2008).
- [10] T. Kondo *et al.*, *Phys. Rev. Lett.* **101**, 147003 (2008).
- [11] D. Hsieh *et al.*, arXiv:0812.2289 (2008).
- [12] H. Ding *et al.*, arXiv:0812.0534 (2008).
- [13] Chang Liu *et al.*, *Phys. Rev. Lett.* **101**, 177005 (2008).
- [14] N. Ni *et al.*, *Phys. Rev. B* **78**, 014507 (2008).
- [15] C. Martin *et al.*, arXiv:0807.0876 (2008).
- [16] M. A. Tanatar *et al.*, arXiv:0812.4991 (2008).
- [17] I. I. Mazin, D. J. Singh, M. D. Johannes and M. H. Du, *Phys. Rev. Lett.* **101**, 057003 (2008).
- [18] J. Dong *et al.*, *Europhys. Lett.* **83**, 27006 (2008).
- [19] T. Nomura *et al.*, *Supercond. Sci. Technol.* **21**, 125028 (2008).
- [20] N. Ni *et al.*, *Phys. Rev. B* **78**, 214515 (2008).
- [21] N. Ni *et al.*, *Phys. Rev. B* **78**, 014523 (2008).
- [22] Neeraj Kumar *et al.*, *Phys. Rev. B* **79**, 012504 (2009).
- [23] G. Wu *et al.*, *J. Phys.: Condens. Matter* **20**, 422201 (2008).
- [24] The exact nature of the pressure-induced superconductivity in CaFe_2As_2 is still under debate. See Milton S. Torikachvili *et al.*, *Phys. Rev. Lett.* **101**, 057006 (2008), A. Kreyssig *et al.*, *Phys. Rev. B* **78**, 184517 (2008) and W. Yu *et al.*, *Phys. Rev. B* **79**, 020511 (2009).
- [25] S. E. Sebastian *et al.*, *J. Phys.: Cond. Matt.* **20**, 422203 (2008).
- [26] N. Harrison *et al.*, arXiv: 0902.1481 (2009).
- [27] A. I. Goldman *et al.*, *Phys. Rev. B* **78**, 100506 (2008).
- [28] Stefan Hüfner, *Photoelectron Spectroscopy*, (Springer-Verlag, Berlin Heidelberg, 1996).
- [29] T. Kondo, Ph.D. Thesis, Nagoya University (2005).
- [30] L. X. Yang *et al.*, *Phys. Rev. Lett.* **102**, 107002 (2009).
- [31] T. Sato *et al.*, arXiv:0810.3047 (2008).
- [32] V. B. Zabolotnyy *et al.*, *Nature* **457**, 569 (2009).
- [33] M. A. Tanatar *et al.*, private communication.